Nitrous oxide quartz-enhanced photoacoustic detection employing a broadband distributed-feedback quantum cascade laser array

Marilena Giglio,[1] Pietro Patimisco,[1,2] Angelo Sampaolo,[1] Andrea Zifarelli,[1] Romain Blanchard,[3] Christian Pfluegl,[3] Mark F. Witinski,[3] Daryoosh Vakhshoori,[3] Frank K. Tittel,[2] and Vincenzo Spagnolo[1,2,a)]

[1]PolySense Lab-Dipartimento Interateneo di Fisica, University and Politecnico of Bari, Via Amendola 173, Bari, Italy
[2]Department of Electrical and Computer Engineering, Rice University, 6100 Main Street, Houston, Texas 77005, USA
[3]Pendar Technologies, 30 Spinelli Place, Cambridge, Massachusetts 02138, USA

We present a gas sensing system based on quartz-enhanced photoacoustic spectroscopy (QEPAS) employing a monolithic distributed-feedback quantum cascade laser (QCL) array operated in a pulsed mode as a light source. The array consists of 32 quantum cascade lasers emitting in a spectral range from $1190 \, cm^{-1}$ to $1340 \, cm^{-1}$. The optoacoustic detection module was composed of a custom quartz tuning fork with a prong spacing of 1 mm, coupled with two micro-resonator tubes to enhance the signal-to-noise ratio. The QEPAS sensor was validated by detecting the absorption of the P- and R-branches of nitrous oxide. The measurements were performed by switching the array QCLs in sequence while tuning their operating temperature to retrieve the fine structure of the two N_2O branches. A sensor calibration was performed, demonstrating a linear responsivity for $N_2O:N_2$ concentrations from 1000 down to 200 parts-per-million. With a 10 s lock-in integration time, a detection sensitivity of less than 60 parts-per-billion was achieved permitting the monitoring of nitrous oxide at global atmospheric levels. *Published by AIP Publishing.*
https://doi.org/10.1063/1.5049872

Numerous optical detection techniques for gas sensing deal with molecules having absorption spectra characterized by well-resolved and separated narrow absorption features. Complex molecule spectra usually lack narrow structures, especially at atmospheric pressure.[1] Molecules with unresolved spectral structures are referred to as broadband absorbers, and their spectral characteristics limit the application of several detection techniques, such as wavelength modulation spectroscopy, which is based on a narrow spectral modulation around an absorption peak.[2]

Broadband spectroscopy would allow for broadband molecule detection, quantitative assessment of the components and their ratios in multi-gas mixtures, and gas temperature variation measurements by monitoring the strength of several rotational-vibrational transitions.

For high resolution spectroscopy of broadband absorbers, laser sources tunable in a wide spectral range are required, such as external cavity quantum cascade lasers (EC-QCLs) or interband cascade lasers (EC-ICLs).[3,4] The external cavity incorporates typically a separate grating for wavelength selectivity.[5] Nevertheless, the mechanical instability of moving parts leads to beam displacement and poor spatial beam quality.[6]

Among mid-IR spectroscopic techniques, Quartz-Enhanced Photoacoustic Spectroscopy (QEPAS) has been demonstrated as one of the most selective, sensitive, compact, robust, and low-cost techniques for trace gas optical detection.[7] In QEPAS, a high quality-factor quartz tuning fork (QTF) is used as a sharp resonator to convert acoustic waves generated by the non-radiative relaxation of the target gas absorbing radiation into an electric signal as a result of quartz piezoelectricity.[8] QEPAS does not require bulky optics: a lens is used to focus the laser beam between the two prongs of the QTF. In contrast to other optical detection techniques such as multi-pass cells or cavity ring-down,[9] QEPAS employs a QTF as a detector, whose responsivity is wavelength insensitive; moreover, the optical alignment is easier and more resilient against imperfect spatial beam quality when the tuning fork is properly designed.[10] These advantages make QEPAS an excellent candidate when broadband sources are used. QEPAS has been demonstrated with an external cavity QCL as a light source exhibiting a frequency tuning of $135 \, cm^{-1}$ with a maximum optical output power of 50 mW.[11] A broadband absorption of Freon 125 (pentafluoroethane) centered at $1208.62 \, cm^{-1}$ was detected, achieving a normalized noise equivalent absorption coefficient of $2.64 \times 10^{-9} \, cm^{-1} \cdot W/Hz^{1/2}$.

In contrast to EC-QCLs which tend to be limited in a full broadband tuning speed to only a few scans per second, the speed and stability advantages of a monolithic array of a distributed-feedback quantum cascade laser (DFB-QCLs) have been demonstrated. In DFB-QCL arrays, each laser is individually addressable to allow for fast purely electrical switching from wavelength to wavelength.[12–15] The unique combination of fast tuning speed, large tuning range, and stability in QCL arrays is a key enabler for fast broadband absorber detection. A single array typically contains 32 individually addressable QCLs; each QCL emits at slightly different wavelengths by design. Several arrays can be further beam-combined into a source with a broader coverage.[13] All

---

a)Author to whom correspondence should be addressed: vincenzoluigi.spagnolo@poliba.it

lasers in an array are fabricated on the same semiconductor chip and do not require any external feedback for lasing or wavelength selection. The emitted wavelength is selected by electrically addressing different lasers, making the process of wavelength tuning inherently fast and reproducible.[13]

In this letter, we report on the development of a nitrous oxide (N_2O) QEPAS sensor based on a monolithic DFB-QCL array composed of 32 individual lasers fabricated on a single QCL chip. The output from individual QCLs is overlapped by using spectral beam combining optics[16] integrated into the laser array package. The laser package, including the QCL chip, a thermo-electric cooler (TEC) for temperature regulation of the array, and the optical elements necessary for beam combining, measures 1 in. $\times$ 2 in. $\times$ 0.5 in. A custom laser driver allows for the individual control of the different lasers within the array, enabling purely electrical tuning of the source by selecting which laser emits at any time. It consists of a single electronic board that measures 6 in. $\times$ 4 in. containing an array of 32 drivers controlled by a Field Programmable Gate Array (FPGA). The lasers are operated in a pulsed mode. Pulsed operation allows for low power consumption and requires no external laser cooling. The lasers can be turned on and off in arbitrary sequences, as long as the duty cycle per laser remains <1%, and the overall array duty cycle is kept below 30%. For each QCL, the drive voltage was set to a value ensuring the highest optical power output. QCL chip temperature is set by a TEC controller (2 in. $\times$ 2 in. electronic board) and can be used to tune the laser center wavelength with a rate of $\sim$0.09 cm^{-1}/°C. The laser driver and TEC controller are operated using the LabVIEW-based software that enables programming of the QCL array sequence and control of temperature tuning. The QEPAS sensor which is schematically depicted in Fig. 1 was tested by measuring two broad absorption bands of N_2O.

The laser beam exiting the array enclosure was spatially filtered by a pinhole and focused between the prongs of a custom quartz tuning fork by means of an antireflection coated ZnSe lens with a focal length of 50 mm. A preliminary investigation of the QCL emission frequency under pulsed excitation was performed by using a Fourier-

transform interferometer in a rapid-scan mode with a resolution of 0.125 cm^{-1}. With 300 ns-wide pulses, all devices exhibit a spectral linewidth of about 1.5 cm^{-1} due to the intra-pulse frequency chirp of the laser during the pulse duration and the potential presence of two longitudinal modes corresponding to the two possible DFB band-edge modes. Smaller linewidths can be obtained with shorter pulses and laser waveguide geometries aimed at suppressing one of the two band-edge modes.[17] The QCL array emission covers a spectral range from 1190 cm^{-1} to 1340 cm^{-1}, with steps of <5 cm^{-1} between adjacent laser devices. This spectral range covers two strong N_2O absorption bands. A pyroelectric camera (mod. Spiricon Pyrocam III-C) with a spatial resolution of 100 μm was placed in the focal plane of the ZnSe lens to acquire and measure the beam profiles of the focused laser spots. Switching between different devices, shifts of the spot center positions of $\sim$100 μm and a collimated beam diameter of $\sim$600 μm were observed. These measurements determine the prong spacing of the tuning fork to be selected. The laser light must not hit the QTF prongs while switching from one QCL to another, otherwise a background signal unrelated to the gas absorption will be generated. For this reason, a custom QTF having a prong spacing of 1 mm with a prong length of 19 mm, a prong width of 1.4 mm, and a crystal thickness of 0.8 mm was selected. Such a QTF showed its best performance when operated at the first overtone flexural mode falling at 25 391.2 Hz at atmospheric pressure[18] with a quality factor of 20 900. The QTF was acoustically coupled with two micro-resonator tubes for pressure wave amplification. The micro-resonator tubes providing the highest signal-to-noise ratio (SNR) enhancement have an internal diameter of 1.52 mm and a length of 5.30 mm and were positioned on-beam, located 200 μm from the QTF.[19] The QEPAS spectrophone composed of the custom QTF and micro-resonator tubes was enclosed in a gas cell, through which the gas flowed at a controlled rate and pressure of 30 sccm and 760 Torr, respectively. The QTF piezocurrent signal was transduced and amplified by a transimpedance amplifier (feedback resistance $R_{fb} = 10$ MΩ) and demodulated by a lock-in amplifier. An external waveform generator was employed to trigger both the laser pulses and the lock-in demodulation at the QTF resonance frequency. The width of the QCL pulses was set at 300 ns which, combined with the operating repetition rate of 25 391.2 Hz, corresponds to a duty cycle of 0.75%, and the lock-in amplifier integration time was set at 100 ms for all measurements.

The QEPAS sensor was validated by detecting the P-branch and the R-branch of nitrous oxide, falling in the 1225–1330 cm^{-1} spectral range. Each branch consists of a series of absorption lines spectrally separated by $\sim$1 cm^{-1}. No Q-branch appears due to selection rules,[1] as shown in the simulation obtained by using the HITRAN database in Fig. 2 (red solid line).[20] The QEPAS measurements were performed by tuning the operating temperature of each QCL from 15 °C to 50 °C in 3 °C steps and switching the lasers in sequence, in order to sweep the overall array spectral range with a resolution of 0.27 cm^{-1}, while a certified concentration of 1000 part-per-million (ppm) N_2O:N_2 is flowing in the gas cell. For each operating temperature, the QCL optical power focused between the QTF prongs was preliminary
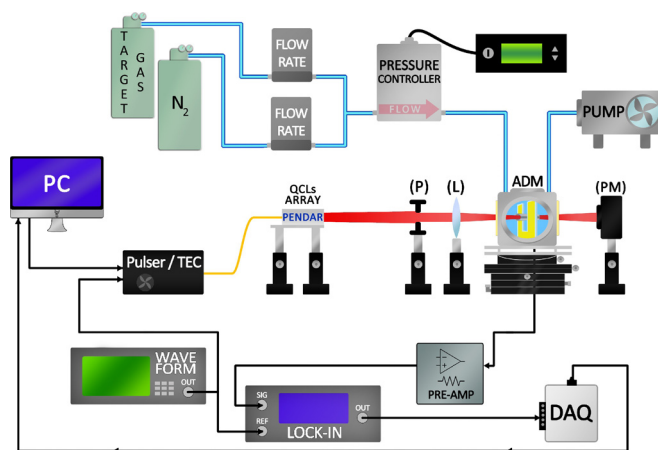

FIG. 1. Schematic of the QEPAS sensor for N_2O detection. P, pinhole; L, lens; ADM, acoustic detection module; PM, power meter; TEC, temperature controller; DAQ, data acquisition board; PC, personal computer. The QCL array was provided by Pendar Technologies.
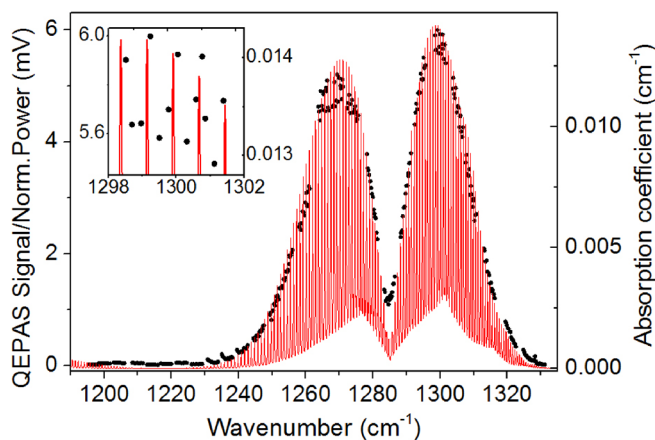
FIG. 2. Comparison between the normalized QEPAS signals scaled to the normalized optical power, measured for a concentration of 1000 ppm $N_2O:N_2$ while tuning the operating temperature of the QCL array (black dots, left y-axis) and the spectrum simulated at the same N_2O concentration by using the HITRAN database (red solid line, right y-axis). Inset: zoom on a narrow spectral range centered at 1300 cm^{-1}.
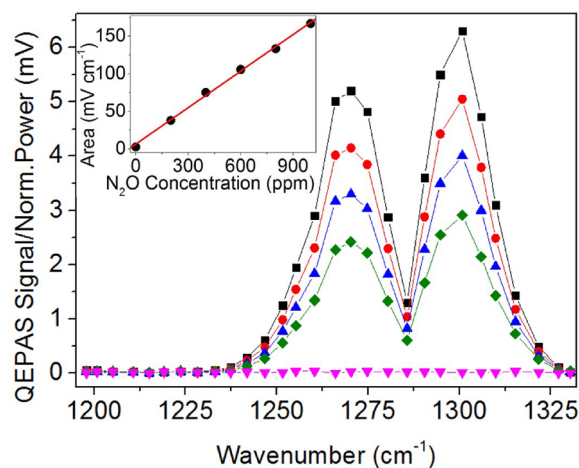

FIG. 3. 1000 ppm (black squares), 800 ppm (red dots), 600 ppm (blue triangles), and 400 ppm (green diamonds) N_2O QEPAS signals normalized by the laser optical power, plotted as a function of the laser peak wavenumber. The operating temperature of the QCL array was fixed at 25 °C. The QEPAS signal measured for pure N_2 (pink triangles) is also reported. Solid lines are visual guides. Inset: The area underneath the QEPAS spectrum in mV·cm^{-1} units measured for each N_2O concentration (black dots) and the corresponding best linear fit (red line).

measured to generate a QCL array normalized optical power curve. The acquired QEPAS signals scaled to this normalized curve are plotted in Fig. 2 (black dots) and compared with the simulated absorption spectrum (red solid line).

The QEPAS measurements exhibit an excellent match with the simulated absorption spectrum in the investigated spectral range, accurately reconstructing the N_2O P- and R-branches centered at 1270 cm^{-1} and 1298 cm^{-1}, with a minimum at 1287 cm^{-1} corresponding to the forbidden Q-branch. The collected data mimic single absorption lines separated by ≈ 1 cm^{-1}, as highlighted in the inset of Fig. 2. By scanning the QCLs and tuning their temperature, we measured comparable signal fluctuations due to photo-thermal induced noise, confirming that the beam alignment is preserved while the array is scanned across its wavelength range by turning on different lasers and tuning of the array temperature. This comes as a result of the use of a beam-combined QCL-array in conjunction with the external pinhole-lens system and the use of a custom QTF with a prong spacing of 1 mm. The time required to produce the spectrum reported in Fig. 2 was 120 min.

Gases with broad absorption features justify the implementation of a rapid scan detection scheme even with a lower resolution in recovering the gas spectrum. To demonstrate this capability, a fast QCL switching mode was tested. In this mode, the QEPAS measurements were performed by operating all devices at a fixed temperature set at 25 °C. The nitrous oxide absorption spectrum was acquired by switching the individual lasers comprising the array sequentially. The acquired QEPAS signals have been scaled by the corresponding measured QCL array normalized optical power curve and are plotted in Fig. 3 (black squares). In this case, the fine structure of the absorption spectrum is no longer distinguishable, but the data obtained reproduce well the envelope of the simulated absorption bands shown in Fig. 2. A trace gas standard generator was used to produce different N_2O concentration levels, using N_2 as the diluting gas and starting from a certified 1000 ppm N_2O in the N_2 mixture. In Fig. 3, the measurements corresponding to 400 ppm, 600 ppm,

800 ppm, and 1000 ppm $N_2O:N_2$ and the signal acquired for pure N_2 are plotted.

The shape of the QEPAS signal is preserved as the N_2O concentration is varied, while its intensity scales linearly with the concentration. For each N_2O concentration, the total measurement time was 8 min, obtained considering $\sim$15 s of QEPAS signal measurements for each QCL.

A calibration curve can be obtained by linearly fitting the area underneath the QEPAS signal curve, as a function of the $N_2O:N_2$ concentration. When targeting 200 ppm $N_2O:N_2$, a total area A of 31.1 mV·cm^{-1} was measured. Comparable 1-σ QEPAS signal fluctuations of $\sim$2 μV were measured for each QCL. By using the law of the propagation uncertainty, the standard deviation of A results in a σ_A = 0.05 mV·cm^{-1} and turns out to be proportional to the 1-σ noise of the QEPAS signal. The resulting signal-to-noise ratio (SNR) is A/σ_A = 622, corresponding to a SNR = 1 minimum detection limit (MDL) = 0.32 ppm. The linear fit between the area underneath the QEPAS signal versus the N_2O concentration yields a slope of 0.16 mV·cm^{-1}/ppm and an intercept of 6.5 mV·cm^{-1}, as shown in the inset in Fig. 3, consistent with the area of 2.6 mV·cm^{-1} measured underneath the curve of the QEPAS background noise level in pure N_2. The calculated R-squared value equals 0.998.

The QEPAS sensor MDL can be further improved by increasing the lock-in integration time. An Allan deviation analysis was performed,[21] predicting the trend of the 1-σ QEPAS signal fluctuations as a function of the lock-in integration time. Based on the proportionality between σ_A and the 1-σ noise, a plot of the MDL as a function of the lock-in integration time was obtained, as shown in Fig. 4.

By averaging the QEPAS signal over longer times, the detection sensitivity decreases to $\sim$60 part-per-billion (ppb) for an integration time of 10 s, thus allowing detection of atmospheric levels ($>$300 ppb) of N_2O.[22]

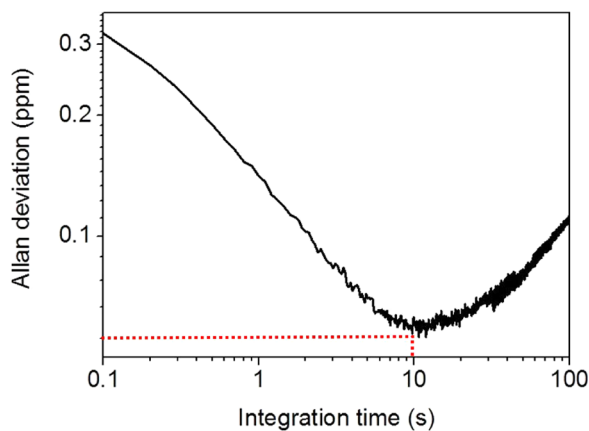In conclusion, we reported on the development of a broadband QEPAS-based sensor for nitrous oxide detection,

FIG. 4. Allan deviation plot of the QEPAS signal in ppm units as a function of the lock-in integration time. For a 10 s integration time, a minimum detection limit of ~60 ppb was achieved (red dashed line).

employing a monolithic distributed feedback-quantum cascade laser array operated in a pulsed mode. N_2O absorption from the P- and R-branches in the $1190 \, cm^{-1}$–$1340 \, cm^{-1}$ spectral range were acquired by tuning the operating temperature of the QCLs and switching of individual devices in sequence. A fast acquisition mode was also demonstrated, allowing for the rapid measurement of gases with broad absorption features. The DFB-QCL array used as the source provided rapid and reproducible tuning with good beam stability in an ultra-compact, low-power package. The use of a custom tuning fork was beneficial to relax alignment tolerances, without compromising detection sensitivity. This study showed the capability and the versatility of QEPAS technique for the detection of broadband absorbers. The employment of the monolithic array of QCLs makes QEPAS a powerful tool to detect absorbers characterized by broad structures, to examine multiple gases and the ratios of various components in a mixture with a single system, and to recognize the presence of contaminant gases altering the spectrum shape and intensity of the primary broadband absorber gas.

[1] G. Herzberg, *Molecular Spectra and Molecular Structure* (Read Books Ltd., 2016), Vol. 1.
[2] L. Consolino, S. Bartalini, H. E. Beere, D. A. Ritchie, M. S. Vitiello, and P. De Natale, Sensors **13**, 3331 (2013).
[3] A. Hugi, R. Maulini, and J. Faist, Semicond. Sci. Technol. **25**, 083001 (2010).
[4] A. Hugi, R. Terazzi, Y. Bonetti, A. Wittmann, M. Fischer, M. Beck, J. Faist, and E. Gini, Appl. Phys. Lett. **95**, 061103 (2009).
[5] D. Caffey, T. Day, C. S. Kim, M. Kim, I. Vurgaftman, W. W. Bewley, J. R. Lindle, C. L. Canedy, J. Abell, and J. R. Meyer, Opt. Express **18**, 15691 (2010).
[6] T. Tsai and G. Wysocki, Appl. Phys. B **100**, 243 (2010).
[7] P. Patimisco, A. Sampaolo, L. Dong, F. K. Tittel, and V. Spagnolo, Appl. Phys. Rev. **5**, 011106 (2018).
[8] A. Sampaolo, P. Patimisco, M. Giglio, L. Chieco, G. Scamarcio, F. K. Tittel, and V. Spagnolo, Opt. Express **24**, 15872 (2016).
[9] I. Galli, S. Bartalini, S. Borri, P. Cancio, D. Mazzotti, P. De Natale, and G. Giusfredi, Phys. Rev. Lett. **107**, 270802 (2011).
[10] A. Sampaolo, P. Patimisco, M. Giglio, M. S. Vitiello, H. E. Beere, D. A. Ritchie, G. Scamarcio, F. K. Tittel, and V. Spagnolo, Sensors **16**, 439 (2016).
[11] R. Lewicki, G. Wysocki, A. A. Kosterev, and F. K. Tittel, Opt. Express **15**, 7357 (2007).
[12] B. G. Lee, M. A. Belkin, R. Audet, J. MacArthur, L. Diehl, C. Pflügl, F. Capasso, D. C. Oakley, D. Chapman, A. Napoleone *et al.*, Appl. Phys. Lett. **91**, 231101 (2007).
[13] M. F. Witinski, R. Blanchard, C. Pfluegl, L. Diehl, B. Li, K. Krishnamurthy, B. C. Pein, M. Azimi, P. Chen, G. Ulu *et al.*, Opt. Express **26**, 12159 (2018).
[14] B. G. Lee, M. A. Belkin, C. Pflügl, L. Diehl, H. A. Zhang, R. M. Audet, J. MacArthur, D. Bour, S. Corzine, G. Höfler *et al.*, IEEE J. Quantum Electron. **45**, 554 (2009).
[15] A. P. Michel, J. Kapit, M. F. Witinski, and R. Blanchard, Appl. Opt. **56**, E23 (2017).
[16] B. G. Lee, J. Kansky, A. K. Goyal, C. Pflügl, L. Diehl, M. A. Belkin, A. Sanchez, and F. Capasso, Opt. Express **17**, 16216 (2009).
[17] F. Capasso, B. G. Lee, C. Pflugl, L. Diehl, and M. A. Belkin, U.S. patent 8,351,481 (8 Januray 2013).
[18] P. Patimisco, A. Sampaolo, L. Dong, M. Giglio, G. Scamarcio, F. K. Tittel, and V. Spagnolo, Sens. Actuator, B **227**, 539 (2016).
[19] P. Patimisco, A. Sampaolo, H. Zheng, L. Dong, F. K. Tittel, and V. Spagnolo, Adv. Phys. X **2**, 169 (2017).
[20] See http://hitran.org/ for HITRAN database.
[21] M. Giglio, P. Patimisco, A. Sampaolo, G. Scamarcio, F. K. Tittel, and V. Spagnolo, IEEE Trans. Ultrason. Ferroelectr. Freq. Control **63**, 555 (2016).
[22] See https://www.epa.gov/climate-indicators/climate-change-indicators-atmospheric-concentrations-greenhouse-gases for checking the levels of major greenhouse gases in the atmosphere.